Chemosphere 309 (2022) 136638

Contents lists available at ScienceDirect

Chemosphere

journal homepage: www.elsevier.com/locate/chemosphere

Cold plasma-assisted regeneration of biochar for dye adsorption

Dharma Raj Kandel [a], Hee-Jun Kim [b], Jeong-Muk Lim [c], Milan Babu Poudel [d], Min Cho [c], Hyun-Woo Kim [e], Byung-Taek Oh [c], Changwoon Nah [a,b], Seung Hee Lee [b,f], Bipeen Dahal [f], Jaewoo Lee [a,b,*]

[a] Department of Bionanotechnology and Bioconvergence Engineering, Jeonbuk National University, 567 Baekje-daero, Deokjin-gu, Jeonju, 54896, Republic of Korea
[b] Department of Polymer-Nano Science and Technology, Jeonbuk National University, 567 Baekje-daero, Deokjin-gu, Jeonju, 54896, Republic of Korea
[c] Division of Biotechnology, Advanced Institute of Environment and Bioscience, College of Environmental and Bioresource Sciences, Jeonbuk National University, Iksan, 54596, Republic of Korea
[d] Department of Convergence Technology Engineering, Jeonbuk National University, 567 Baekje-daero, Deokjin-gu, Jeonju, 54896, Republic of Korea
[e] Department of Environmental Engineering, Division of Civil, Environmental, Mineral Resource and Energy Engineering, Soil Environment Research Center, Jeonbuk National University, 567 Baekje-daero, Deokjin-gu, Jeonju, 54896, Republic of Korea
[f] Department of Nano Convergence Engineering, Jeonbuk National University, 567 Baekje-daero, Deokjin-gu, Jeonju, 54896, Republic of Korea

HIGHLIGHTS

- Carbonized rice husk (CRH) was used for adsorption-based removal of dye molecules.
- The adsorption kinetics was governed by the pseudo-second-order model.
- Cold plasma (CP) treatment successfully regenerated the dye-adsorbed CRH.
- CP treatment was workable for the five consecutive adsorption tests of the used CRH.
- The regeneration mechanism was discussed in detail based on thorough analyses.

GRAPHICAL ABSTRACT

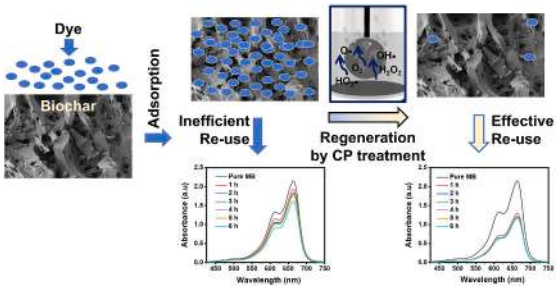

ARTICLE INFO

Handling Editor: CHANG MIN PARK

Keywords:
Biochar
Methylene blue
Cold plasma
Adsorption
Regeneration

ABSTRACT

Environmental remedies, including adsorption-based water purification, are now being asked to meet the requirement for a low-carbon circular economy requiring low energy and low material consumption. In this regard, we tested the possibility of regenerating adsorbents *via* cold plasma (CP) treatment for less use of adsorbents and no washing solution. In the adsorption of methylene blue (MB) using carbonized rice husk (CRH) and five successive regeneration cycles by CP treatment, the removal efficiencies were maintained at a moderate level (~70% of the initial performance), unlike five consecutive adsorption without CP treatment (~9–13% of the initial performance). The regeneration of CRH by CP treatment was also double-checked by the FESEM, EDS, BET, FTIR, XPS, and surface zeta potential measurements. The successfully recovered adsorption capability is related to the remediation of adsorption sites. It is also worth noting that the required power consumption for recycling by CP treatment was about 6.4 times lower than carbonizing new rice husks. This work provides insights into recovering adsorbents using CP without rigorous, costly, and energy-intensive processes.

* Corresponding author. Department of Bionanotechnology and Bioconvergence Engineering, Jeonbuk National University, 567 Baekje-daero, Deokjin-gu, Jeonju, 54896, Republic of Korea.
E-mail address: jaewoolee@jbnu.ac.kr (J. Lee).

https://doi.org/10.1016/j.chemosphere.2022.136638
Received 18 July 2022; Received in revised form 19 September 2022; Accepted 25 September 2022
Available online 29 September 2022

1. Introduction

Synthetic dyes are widely used in a variety of industries such as cosmetic, paper, paint, leather, fur, and textile manufacturing industries (Kim et al., 2022; Radoor et al., 2022). Out of many dyes, methylene blue (MB) is one of the most commonly used cationic dyes in chemical industries for analytical purposes and in the textile industry to dye wools, silk, and cotton (Kim et al., 2014; Toriello et al., 2020; Radoor et al., 2021b). In spite of its great versatility in various applications, long-term exposure to MB causes skin irritation, breathing difficulty, mental confusion, nausea, vomiting, and diarrhea (Santoso et al., 2020). Therefore, the removal of MB from water sources is necessary to guarantee our health and safety while preserving an aqueous environment. Among various water and wastewater treatment processes to handle dye pollutants (Nie et al., 2020; Toriello et al., 2020; Ibrahim et al., 2021; Li et al., 2022; Mahmoudi et al., 2022), adsorption is one of the most promising and effective methods to remove MB from contaminated water because of its beneficial features such as easy operation, low cost, higher efficiency, and recyclability (Jun et al., 2020a; Jun et al., 2020b; Radoor et al., 2021a; Nandi et al., 2022).

For MB removal, carbon materials and transition metal compounds (*e.g.,* TiO_2, MnO_2, $MnTiO_3$, WO_3, Fe_3O_4, $La_2O_2CO_3$, and $ZnFe_2O_4$, *etc.*) have generally been applied for adsorption and adsorption/degradation of MB molecules, respectively (Xing et al., 2011; Li et al., 2016; Sethunga et al., 2019b; Alkaykh et al., 2020; Poudel et al., 2020). Although transition metal compounds are benchmark catalysts for MB removal, these materials are difficult to regenerate and remain secondary pollutants in the water treatment system (Naushad et al., 2019). On the other hand, carbon-based adsorbents are free from the regeneration issue in that they are inert to regenerating agents, making them more readily available for dye removal. Among several carbon-based adsorbents, people have started paying attention to biochar adsorbents obtainable from agro–wastes due to the high specific surface area, low cost, abundant availability, and eco-friendly nature (Ahmad et al., 2020). This fact indicates that agro-waste based adsorbents meet the requirements (*e.g.,* high adsorption capacity and recyclability (Babu Poudel et al., 2022)) for excellent adsorbents. As a result, numerous carbon sources such as rice husks and straw, barley husk, sugarcane bagasse, orange peel, coconut bagasse, papaya peels, bamboo dust, furniture waste char, groundnut shell, walnut shell, almond shell, apricot stone, *etc.* have been frequently used as biochar adsorbents for the removal of MB in the last decade (Godlewska et al., 2017; Santoso et al., 2020; Lim et al., 2021).

More importantly, we can facilitate the transition to a low-carbon circular economy by utilizing agro-waste based adsorbents as waste-to-resource strategies, which is consistent with the recent movement toward carbon neutrality. To attain carbon neutrality, we have to reduce the amount of carbon used for energy production in all areas (Lee and Lim, 2021), which can be promoted by cutting down on using or producing new products by recycling agro-waste based adsorbents. With this in mind, recycling adsorbents can be pursued *via* various methods such as chemical, steam, thermal, and biological regeneration (Ferro--Garcia et al., 1996; Küntzel et al., 1999; Ng et al., 2009; Guo et al., 2020). Among the several recycling methods, chemical regeneration using HNO_3, H_2SO_4, HCl, NaOH, and ethanol (Lu et al., 2011; Naushad et al., 2019; Kim et al., 2022) has been preferred and widely used since it is faster than biological approach while causing lower mass loss than thermal regeneration. For example, chemical agents such as NaOH, HCl, and H_2O_2 have been implemented alone or in combined forms depending on their efficiency in recovering the used adsorbents (Rethinasabapathy et al., 2022). When it comes to other examples using the mixture of chemical agents, Ghaedi et al. used the mixture of ethanol and NaCl to recycle the modified mine silicate waste (Ghaedi et al., 2022).

However, the aforementioned practical applications of chemical regeneration methods are limited because of the high cost (Kurbus et al., 2002) and complex operation process (Zhang et al., 2022). Even worse, chemical regeneration using acid/base, electrolytes, or organic/inorganic solvents inevitably leaves more hard-to-manage wastewater behind because organic foulants persistently exist in the regenerating chemicals after being detached from adsorbents during chemical regeneration (Kim et al., 2022). Another problem is that chemical regeneration is typically accompanied by the separation of regenerated adsorbents from the regenerating chemicals, increasing the load of the process. In contrast, an advanced oxidation process (AOP) can be considered an alternative in that it is free from the problems imposed by high cost, high energy consumption, and complex operation of chemical regeneration while it is effective in removing adsorbed organic foulants onto adsorbents and thereby regenerating used adsorbents without persistent residual foulants behind the removal process. Indeed, AOPs using UV-light, H_2O_2, and Fenton reactions were reported to be effective in mediating the regeneration of saturated carbon (Santoso et al., 2020).

Among various AOPs, cold plasma (CP) treatment can be considered one of the more suitable alternatives to the adsorbent's regeneration due to its several strengths such as lower energy consumption along with faster and more efficient oxidation at room temperature and atmospheric pressure independently of pH, turbidity, and the content of organic foulants, unlike other AOPs (Kim et al., 2020, 2021, 2022; Lv et al., 2020). Since MB is converted into NO_3^-, SO_3^{2-} or SO_4^{2-}, and H_2O after the degradation by CP treatment, it is possible to remove the adsorbed organic foulants onto adsorbents with lower energy consumption without persistent residual foulants behind the adsorbent's regeneration process. Furthermore, CP treatment could be more appropriate for the adsorbent's regeneration than for directly oxidizing organic foulants in water on a large scale. To be specific, if organic foulants are widely dispersed or dissolved in a bulk solution at a large scale, it should require a long time for direct oxidation by CP treatment to treat the foulants. Considering that the primary oxidants such as hydroxyl (OH·), hydroperoxyl (HO_2·), oxygen (O·), nitric oxide (NO·), and nitrogen dioxide (NO_2·) radicals along with ozone (O_3) and hydrogen peroxide (H_2O_2) generated by CP processes (Jia et al., 2018; Lee et al., 2021) are known to have a short life span (Brisset and Pawłat, 2015; Kazemi and Taghvaei, 2021), direct oxidation could be inappropriate at a large scale. On the other hand, the oxidation of the adsorbed foulants onto adsorbents can drastically improve the usability of the radical species supplied by CP treatment in that adsorption could confine organic foulants to a small and limited space (*i.e.,* adsorbents), thereby remarkably reducing a working volume and facilitating radical species to actual oxidation of foulants. Nevertheless, no work has focused on regenerating used adsorbents using CP treatment.

With this in mind, we propose a novel approach to regenerate carbonized rice husks (CRHs) simultaneously using a CP treatment method. First, adsorption experiments were carried out to test the feasibility of CP treatment for biochar regeneration. Then, their adsorption kinetics and isotherms were studied in detail before and after the adsorbent's regeneration. Also, FTIR, FESEM–EDS, and XPS characterizations were conducted to dig deeper into the MB adsorption by CRH and the regeneration of the used CRH by CP treatment. Finally, the percentage removal of the regenerated CRH was calculated during consecutive adsorption tests after every regeneration. It was found that CRH maintained the adsorption capacity at a comparable level to the first adsorption even after successive regeneration processes. We hope this work provides a new perspective for the efficient regeneration of adsorbents by CP treatment while avoiding the formation of secondary pollutants in the effluents.

Fig. 1. Schematic representation for the MB adsorption and regeneration of CRH by CP treatment.

2. Materials and methods

2.1. Preparation of CRH

Rice husk was obtained from a farm in Iksan, Korea. Rice husk was washed with deionized (DI) water several times and dried in a vacuum oven (DF-3.5, Daeheung Science, Incheon, Korea) with a maximum output power of 3.6 kW at 70 °C for 3 days. During the drying process, the mass of rice husk was decreased by 17% while losing moisture. Subsequently, 20 g of dried CRH was carbonized at 650 °C for 3 h at the ramping rate of 10 °C min^{-1} under N_2 atmosphere. The obtained percentage yield after the carbonization was about 36%. The as-prepared CRH was identified to possess favorable structural characteristics (*e.g.,* amorphous structure) and composition (*e.g.,* silica and mineral ash) for adsorption (Fig. S1, See more details in Supplementary Information).

2.2. Characterization of CRH samples

The initial, used, and regenerated CRHs were characterized to determine the changes in the physicochemical properties of CRH after adsorption and regeneration. The specific surface area and pore textural properties were examined by N_2 adsorption-desorption using Brunauer-Emmett-Teller (BET; Micromeritics, ASAP 2020, USA) at 77K. The functional groups and peak intensities of the initial, used, and regenerated CRHs were analyzed by Fourier transform infrared (FTIR) spectrometer (Frontier, PerkinElmer, USA). The presence of MB on three types of CRHs was analyzed by X-ray photoelectron spectroscopy (XPS; Nexsa XPS system, Thermo Fisher Scientific, UK) using monochromatic Al-Kα (1486.6 eV). The surface images and elemental analyses of CRH before and after adsorption were observed by a field emission scanning electron microscopy (FESEM, Carl Zeiss, SUPRA40VP, Oberkochen, Germany) and energy dispersive X-ray diffraction spectroscopy (EDS) placed at the Center for University-Wide Research Facilities (CURF) after sputter-coated with platinum for 90 s. The crystallinity of the prepared CRH was identified by X-ray diffraction (XRD) (D8 Advance, Bruker, Germany). The surface zeta potential of biochars was determined by the Zetasizer (ZEN3600, Zetasizer Nano ZS, UK).

2.3. Adsorption experiment

Prior to adsorption experiments, the removal efficiencies of the initial CRH were compared at different concentrations of MB, and 10 ppm was chosen as an optimized concentration to evaluate the adsorption performance of CRH (Fig. S2). Accordingly, the rest of the adsorption experiments were performed at 10 ppm and 20 ppm. To assess the adsorption capacity and initial removal efficiency of CRH, the adsorption experiments were carried out using 100 mL of a 10 ppm aqueous MB (Sigma Aldrich, USA) solution along with 100 mg of CRH for 6 h. The solution's pH was adjusted using 0.1 M HCl and 0.1 M NaOH. A UV–visible spectrophotometer (SP-UV1100, DLAB, China) was used in order to determine the MB concentration after adsorption. The adsorption capacities (Q, mg g^{-1}) and percentage removal (%R) were determined by the following equations:

$$Q = \frac{C_i - C_f}{m} \times V \quad (1)$$

$$\%\,R = \frac{C_i - C_f}{C_i} \times 100 \quad (2)$$

where C_i (mg L^{-1}) and C_f (mg L^{-1}) are the initial and final concentrations of MB, V (L) is the volume of an MB solution, and m (mg) is the mass of CRH. Meanwhile, the pseudo-second-order kinetics was employed to study the adsorption kinetics based on the following relationship.

$$\frac{t}{Q_t} = \frac{1}{K_2 Q_e^2} + \frac{t}{Q_e} \quad (3)$$

where t is the adsorption time in minutes, K_2 is the rate constant for the second-order reaction, and Q_e (mg g^{-1}) and Q_t (mg g^{-1}) are the adsorption capacity at equilibrium and a certain time 't', respectively.

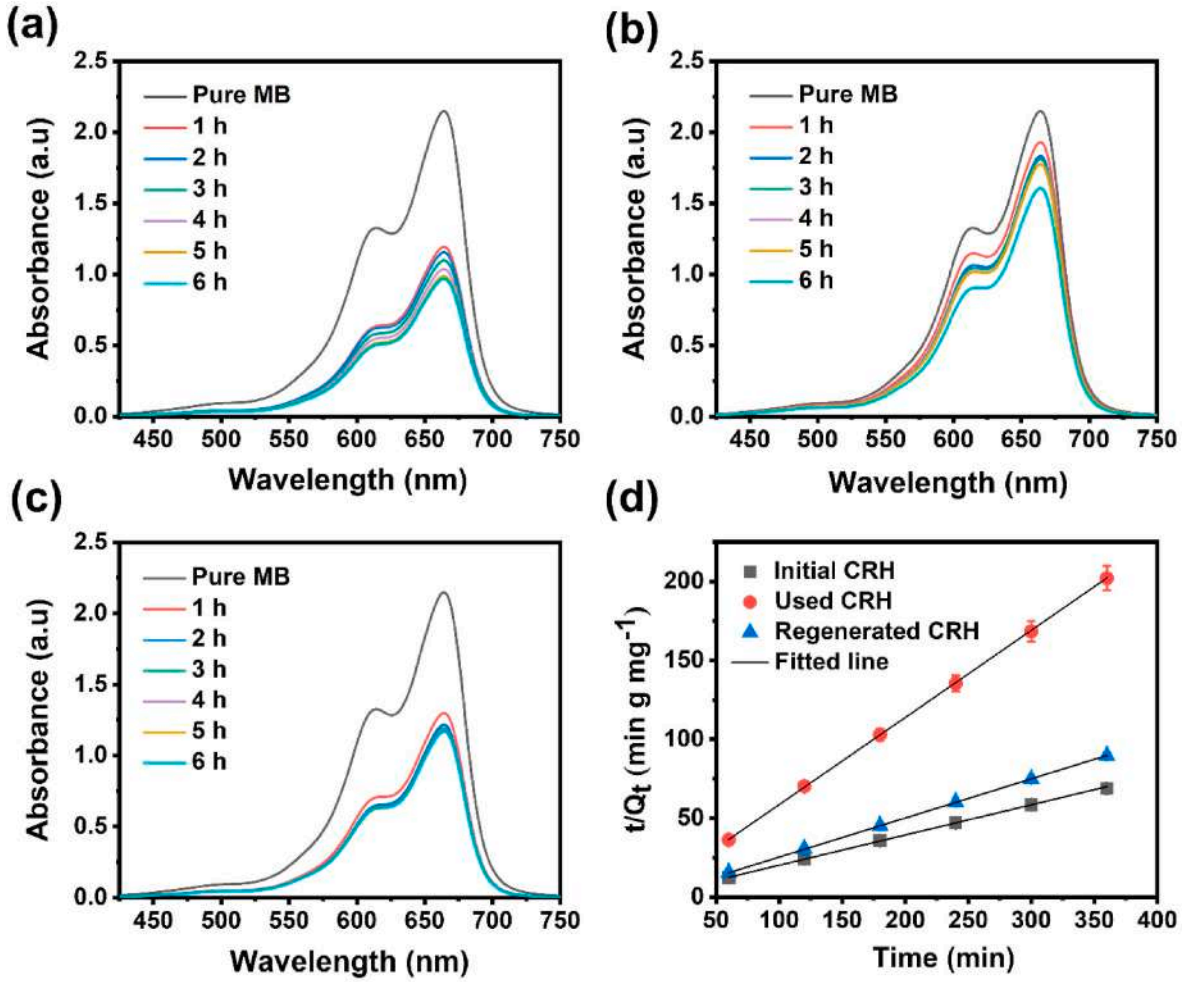

Fig. 2. UV absorbance spectra of the (a) initial, (b) used, and (c) regenerated CRH obtained during dye removal at different times. (d) Fitting for the kinetic plot of t versus t/Q_t. Error bars mean the standard deviation obtained from three different adsorption tests.

Table 1
Parameters for the pseudo-second-order model for CRH.

Sample	Parameters		
	Q_e (mg g^{-1})	K_2 (g mg^{-1} min^{-1})	R^2
Initial CRH	5.23	5.21×10^{-2}	0.99982
Used CRH	1.81	8.60×10^{-2}	0.9993
Regenerated CRH	4.03	9.62×10^{-2}	0.9996

2.4. Regeneration

After the adsorption, the CRH residue was thoroughly rinsed with DI water and left to dry at room temperature overnight. After complete drying, the used CRH was added to 100 mL of DI water and subsequently exposed to the air containing radical species (*e.g.,* $HO_2\cdot$, $OH\cdot$, $O_2\cdot$, or their recombination (Zeghioud et al., 2020; Sivakumar and Lee, 2022)) generated by CP at 10 mA and 2.2 W for 1 h to remove the adsorbed dye molecules (Fig. S3, See more details on the possible pathways of MB degradation in Supplementary Information). The radical species were created by a lab-scale CP system (Groon Co., Ltd., Jeonju, Korea) and supplied to the CRH mixture at 5 L min^{-1} from an air pump (Shinhwahightech, ZP-25, Chungju, Korea) at 19 W. The regeneration condition was taken from the literature addressing the optimization for the generation of plasma species (Lee et al., 2018). Fig. 1 demonstrates the schematic representations for the adsorption and regeneration processes of the CRH by CP treatment. The regeneration efficiency of CP treatment

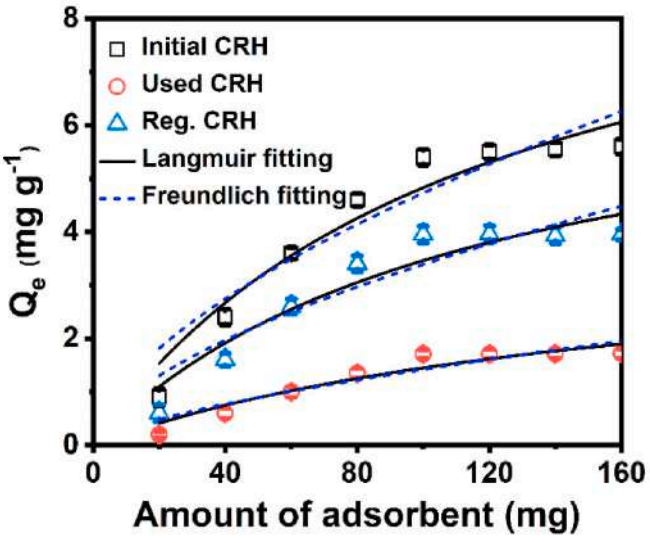

Fig. 3. Isotherm study for MB adsorption by the initial, used, and regenerated CRHs.

Table 2
Parameters of the isotherm models for MB adsorption by the initial, used, and regenerated CRHs.

Isotherm models	Parameters	Adsorbents		
		Initial CRH	Used CRH	Regenerated CRH
Langmuir	q_m (mg g^{-1})	10.8	3.89	7.49
	K_L (L mg^{-1})	0.0077	0.0059	0.0086
	R^2	0.918	0.911	0.908
Freundlich	K_F ((mg g^{-1})(mg L^{-1}))$^{1/n}$	0.27	0.05	0.19
	n	0.61	0.70	0.62
	R^2	0.884	0.871	0.851

was calculated by the following equation (Narbaitz and Cen, 1997; Narbaitz and Karimi-Jashni, 2009; Salvador et al., 2015).

$$\text{Regeneration efficiency } (\%) = \frac{q_r}{q_i} \times 100 \quad (4)$$

where q_i and q_r are the CRH's adsorption capacities at equilibrium before (*i.e.,* initial CRH) and after the regeneration of CRH (*i.e.,* regenerated CRH). For the consecutive removal efficiency and regeneration test, we used 250 mg of CRH along with 250 mL of 10 and 20 ppm MB solutions and monitored the removal efficiencies for 8 h, followed by the regeneration by CP for 1 h supplying the air including radical species at 5 L min^{-1}.

3. Results and discussion

3.1. Kinetics of MB adsorption by the initial, used, and regenerated CRHs

The adsorption kinetics (60–360 min) were studied for the initial, used, and regenerated CRHs samples in order to determine their adsorption performance and regeneration efficiency of CP treatment. As shown in Fig. 2(a), the initial CRH demonstrated a desirable adsorption capacity of 5.23 mg g^{-1} for the MB, which is similar to the performance reported in the previous literature (Han et al., 2007; Chowdhury et al., 2009; Yan et al., 2016; Hummadi et al., 2022). After once-used CRH was rinsed only with DI water, the used CRH's adsorption capacity was significantly reduced to 1.81 mg g^{-1} (Fig. 2(b)). This result infers that rinsing with DI water was not enough to fully regenerate the used CRH's adsorption capacity. In contrast, the regenerated CRH by CP treatment exhibited that its adsorption capacity of 4.03 mg g^{-1} was maintained at a comparable level (Fig. 2(c)).

To gain a deeper insight into the adsorption kinetics, the pseudo-second-order model was employed for quantitative comparison. From the calculations, the experimental data were best fitted with the linearized pseudo-second-order model (Fig. 2(d)). The rate constant (K_2), regression coefficient (R^2), and adsorption capacity (Q_e) for the initial, used, and regenerated CRHs were calculated and presented in Table 1. The values of R^2 were close to 1 for all the cases, implying that the adsorption kinetics is governed by the pseudo-second-order model. Generally, if adsorption kinetic data were well fitted with the pseudo-second-order model, the adsorption is known to be controlled by chemisorption due to the adsorbent-adsorbate interaction as a rate-determining step rather than mass transfer (Albadarin et al., 2017; Panão et al., 2019; Fang et al., 2021). As conventional wisdom suggests, chemisorption could occur in the MB adsorption using CRHs, considering that the prepared CRH contained adsorption sites consisting of silica or oxygen-functional groups capable of bringing about electrostatic attractions of cationic MB molecules. Note that chemisorption typically involves both covalent bond sharing electrons and ionic bond exchanging electrons (*e.g.,* electrostatic attraction) between adsorbent and adsorbate (Wu et al., 2022).

More importantly, the higher Q_e value of the regenerated CRH than the used CRH signifies that many sites available for adsorption on the CRH were successfully regenerated by CP treatment. On the contrary, a significant area of the adsorption sites on the used CRH was estimated to be occupied by the previously adsorbed dyes, ending up aggravating the adsorption capacity of the used CRH. From the above analysis, we could draw a conclusion that CP treatment effectively regenerated the used CRH by removing the pre-adsorbed dyes and rehabilitating the adsorption sites while rinsing with DI water just partially detached the adsorbed dyes and thus was not enough to fully regenerate the used CRH.

3.2. Isotherm study for MB adsorption by the initial, used, and regenerated CRHs

Apart from the pseudo-second-order model, the isotherm study for MB adsorption by the initial, used, and regenerated CRHs was performed by varying the amount of the adsorbents (20–160 mg) to further verify whether the regenerated CRH possesses a comparable adsorption capacity to the initial CRH, unlike the used CRH. Two adsorption isotherm models, namely Langmuir and Freundlich, were used to investigate the adsorption processes based on equations (5) and (6), respectively (Poudel et al., 2021).

$$\mathbf{Q_e} = \frac{\mathbf{q_m K_L C_e}}{\mathbf{1 + K_L C_e}} \quad (5)$$

$$\mathbf{Q_e} = \mathbf{K_F C_e}^{\mathbf{1/n}} \quad (6)$$

where Q_e (mg g^{-1}) is the adsorption capacity at equilibrium, q_m (mg g^{-1}) is the maximum adsorption capacity, C_e (mg L^{-1}) is the adsorbate concentration at equilibrium, K_L (L mg^{-1}) is the Langmuir constant related to the adsorption energy, and K_F ((mg g^{-1})(mg L^{-1}))$^{1/n}$ and n are Freundlich constants related to the adsorption capacity and adsorption intensity, respectively. The nonlinear fitting for the MB adsorption by the initial, used, and regenerated CRHs was provided in Fig. 3 along with the detailed nonlinear regression parameters (Table 2). The adsorption capacities for all the adsorbents elevated sharply with an increase in the amount of adsorbent and progressively achieved equilibrium. However, the adsorbent particles appeared to agglomerate as the adsorbent dose went beyond 100 mg, decreasing the adsorption sites and adsorption capacity, as described in the previous literature (Brice et al., 2021). This phenomenon can also be explained in terms of overlapping or aggregation of adsorption sites and the resulting reduction in the available specific surface area at a higher amount of adsorbent (Srivastava et al., 2008). The nonlinear fitting occurring due to the agglomeration at a higher concentration of CRH demonstrated that the correlation coefficient (R^2) for the Langmuir model was best fitted for all types of the CRHs (Table 2), suggesting monolayer adsorption of MB (Mpatani et al., 2020).

More importantly, according to Table 2, the used CRH's maximum adsorption capacity was around one-third of the initial CRH's one or smaller than that, whereas the regenerated CRH's adsorption capacity was recovered at about 70% of the initial one. This significant difference between the adsorption capacities of the used and regenerated CRHs is estimated to result from the adsorption sites properly regenerated by CP treatment, as discussed in Section 3.1. To confirm whether the comparable adsorption capacity of the regenerated CRH stemmed from the rehabilitated adsorption sites by CP treatment, the BET characterization (Fig. 4) was carried out in order to determine the changes in the adsorption sites by the MB adsorption and CP treatment. As shown in Table 3, the used CRH exhibited a much smaller specific surface area and pore volume than the initial CRH, which is attributed to the surfaces and pores occupied by MB molecules. In stark contrast, the regenerated CRH's specific surface area and pore volume were kept at around 75% of the initial CRH, obviously supporting our previous hypothesis that CP treatment effectively removed the adsorbed MB molecules and

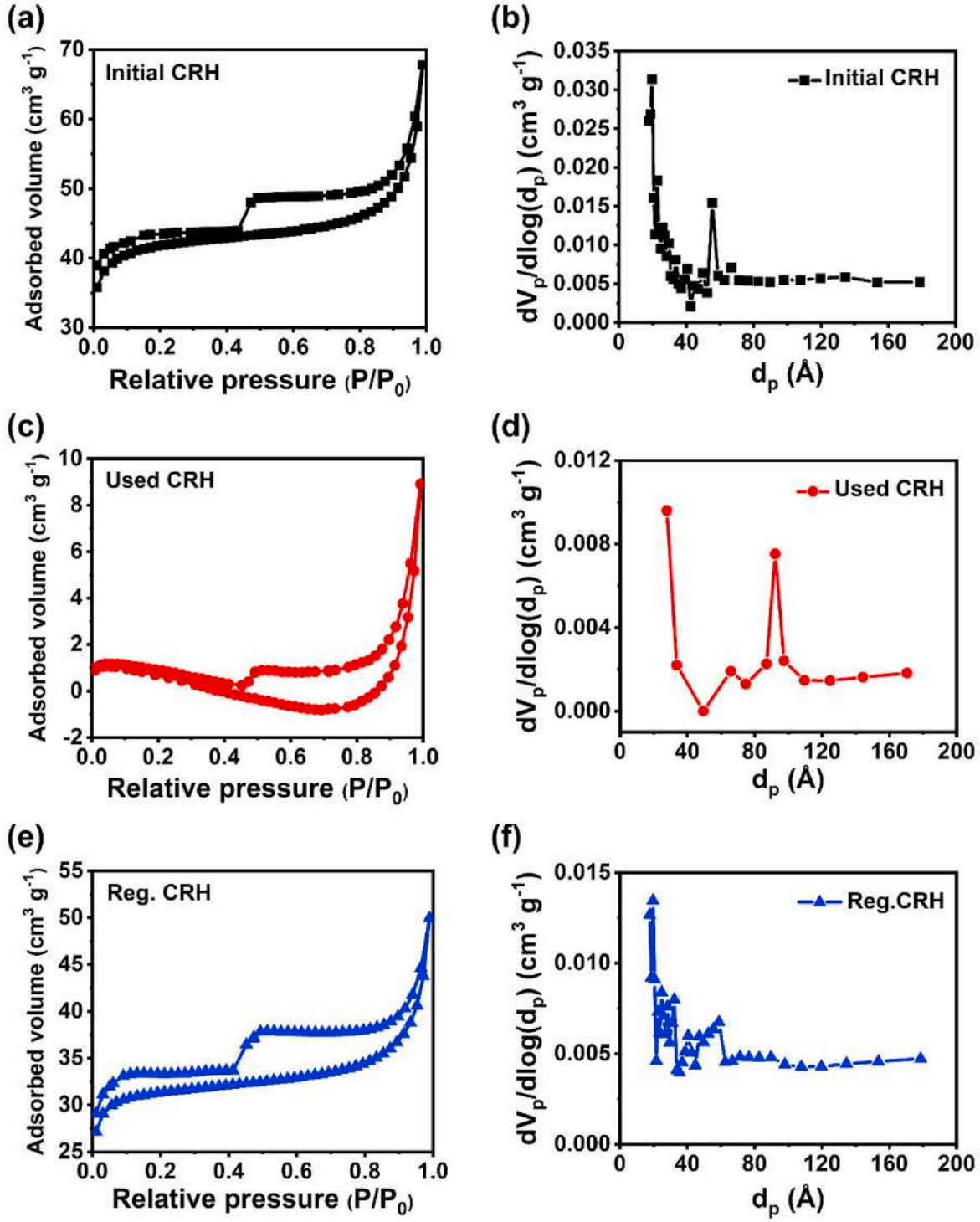

Fig. 4. N_2 adsorption-desorption isotherms and BJH plots for (a, b) initial, (c, d) used, and (e, f) regenerated CRH.

Table 3
Specific surface area and average pore volume obtained from the BET analysis.

Samples	BET surface area ($m^2\ g^{-1}$)	Average pore volume ($cm^3\ g^{-1}$)
Initial CRH	161	0.104
Used CRH	4.37	0.017
Regenerated CRH	124	0.077

successfully regenerated the used CRH.

3.3. *Further investigations to dig deeper into the changes occurring during MB adsorption and CRH regeneration*

The FTIR spectra of the initial, used, and regenerated CRHs were obtained in order to determine the change in the surface functional properties of CRH before and after regeneration (Fig. 5). First, the most eye-catching peaks in the initial CRH were the multiple peaks at 400–1100 cm^{-1} (Fig. 5(a)) assigned to the Si-related functional groups

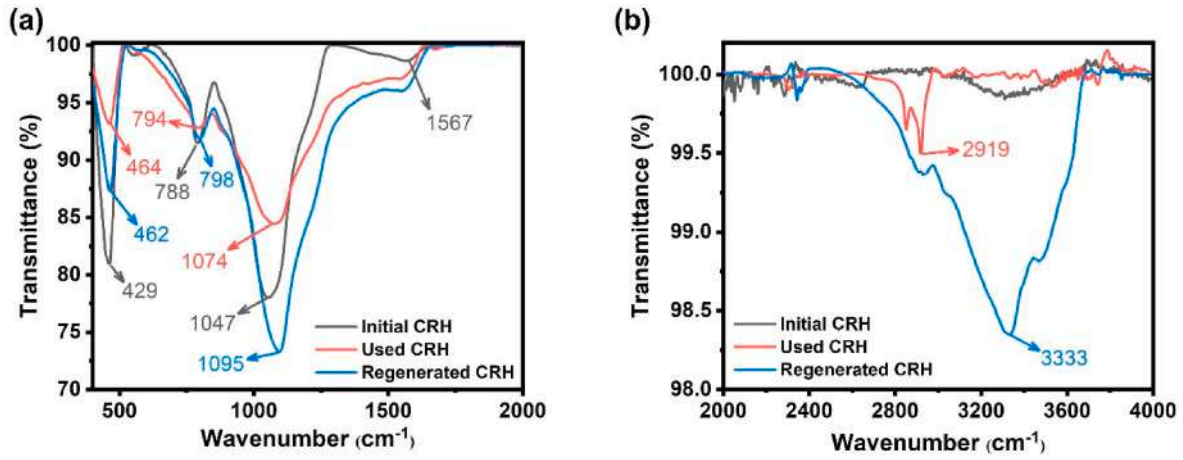

Fig. 5. FTIR spectra of the initial, used, and regenerated CRHs.

Table 4
Peak assignments of the IR active vibrations of the initial, used, and regenerated CRHs along with MB.

Sample	Frequency (cm^{-1})	Assignment	Ref.
Initial CRH	429	Stretching of vibration mode of Si–O	Nemaleu et al. (2021)
	788	Si–O–C stretching vibration	Bakdash et al. (2020)
	1047	Asymmetric stretching vibration of Si–O–Si	You et al. (2021)
	1567	C=C vibration in aromatic rings	Patawat et al. (2020)
Used CRH	462	Si–O–Si bending vibration	Adam et al. (2013)
	794	CH3 rocking in Si–CH_3	Sethunga et al. (2019a)
		Deformation and bending modes of Si–O–Si	Adam et al. (2013)
	1074	Si–O–Si stretching	(Adam et al., 2013; Sethunga et al., 2019a; Bakdash et al., 2020)
	2919	C–H stretching vibration of the methyl group of MB	Phan et al. (2017)
Regenerated CRH	464	Si–O–Si bending vibration	Adam et al. (2013)
	798	CH3 rocking in Si–CH_3	Sethunga et al. (2019a)
		Si–O bending	Bakdash et al. (2020)
		Deformation of Si–O–Si	Adam et al. (2013)
	1095	Asymmetric stretching vibration of Si–O–Si	You et al. (2021)
		C–O stretching in alcohols, esters, phenols, and carboxyl acids	Patawat et al. (2020)
		Aromatic C–H in-plane deformation	Patawat et al. (2020)
	3333	-OH group	Hu et al. (2008)

(Bakdash et al., 2020; Nemaleu et al., 2021; You et al., 2021) listed in Table 4. It is evident from these FTIR peaks that the initial CRH contained silica capable of adsorption. Next, the used CRH's FTIR peak assigned at 2919 cm^{-1} (Fig. 5(b)), which represents the C–H stretching vibration of the methyl group of MB (Phan et al., 2017), also supports that the initial CRH containing silica successfully adsorbed MB dye molecules. Note that the peak at 2919 cm^{-1} appeared in the used CRH's FTIR spectrum, whereas it was not observed in the initial CRH's one.

Meanwhile, the peaks assigned to the Si-related functional groups (Adam et al., 2013; Sethunga et al., 2019a; Bakdash et al., 2020; You et al., 2021) were also observed in the used and regenerated CRHs (Fig. 5 (a)), demonstrating that silica persistently existed even though it went through adsorption and CP treatment. This fact signifies that we could keep utilizing silica in the prepared CRH for adsorption if we regenerate the used CRH by removing the adsorbed dye molecules *via* CP treatment. More intriguingly, the intensity of the peak assigned at 1095 cm^{-1} became more prominent in the regenerated CRH than in the initial CRH. The increase in the regenerated CRH's peak intensity at 1095 cm^{-1} is thought to stem from the additional contribution by the oxidation of the used CRH by CP treatment, given that the peak at 1095 cm^{-1} is also assigned to the aromatic C–H in-plane deformation and C–O stretching (Patawat et al., 2020). In other words, the increased peak intensity at 1095 cm^{-1} could be evidence demonstrating that the used CRH was adequately oxidized by CP treatment. Another evidence of the used CRH's oxidation is the –OH group at 3333 cm^{-1} (Hu et al., 2008), which appeared after CP treatment (Fig. 5(b)). The OH peak also strongly suggests that the used CRH was oxidized by CP treatment generating hydroxy radicals. However, it does not necessarily mean that the changes in the FTIR peaks assigned at 1095 and 3333 cm^{-1} also prove the removal of MB molecules adsorbed onto the used CRH by CP treatment (*i.e.,* regeneration of the used CRH) because the peak assigned to the methyl group of MB (2919 cm^{-1}) overlaps the broad OH peak (Fig. 5(b)), blurring the distinction between the persistent presence and removal of MB.

For that reason, the XPS spectra of the initial, used, and regenerated CRHs have been additionally investigated to further verify the removal of the adsorbed MB molecules onto the used CRH and the resulting regeneration of the used CRH. As shown in Fig. 6(a), the peak intensity of the N 1s spectrum for the used CRH was relatively very high, which is due to the MB adsorbed on the used CRH. On the other hand, the peak intensity was significantly reduced for the regenerated CRH, signifying that the adsorbed MB molecules were removed after CP treatment. Similar trends can be observed in the S 2p HRXPS spectra (Fig. 6 (b)) and the surface zeta potential measurements (Fig. S4, See more details in the Supplementary Information). Furthermore, FESEM analysis and EDS mapping were performed to examine the elemental distribution of C, O, Si, N, and S of the used and regenerated CRHs to double-check the MB removal by CP treatment. FESEM images (Fig. 7(a)-7(c)) revealed that all types of CRH were porous in macroscopic morphologies. Also, the porous structure was maintained while the prepared CRH experienced adsorption and CP treatment, implying that the CRH's adsorption capacity is less likely to change significantly due to structural variation. Meanwhile, the EDS mapping and corresponding EDS spectra analysis revealed the presence of N and S after MB adsorption (Fig. 7(d)), which

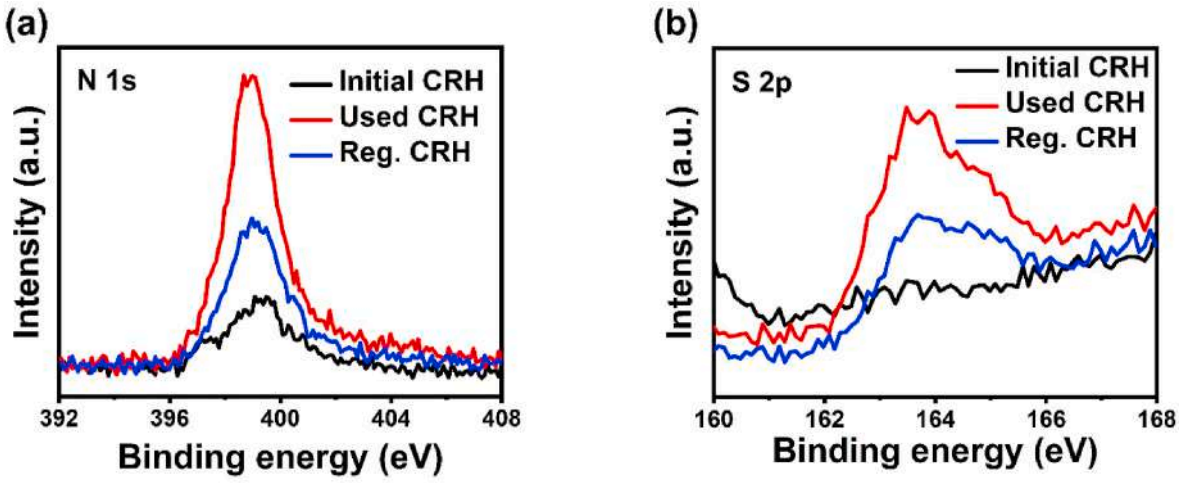

Fig. 6. HRXPS spectra for (a) N 1s and (b) S 2p for the initial, used, and regenerated CRHs.

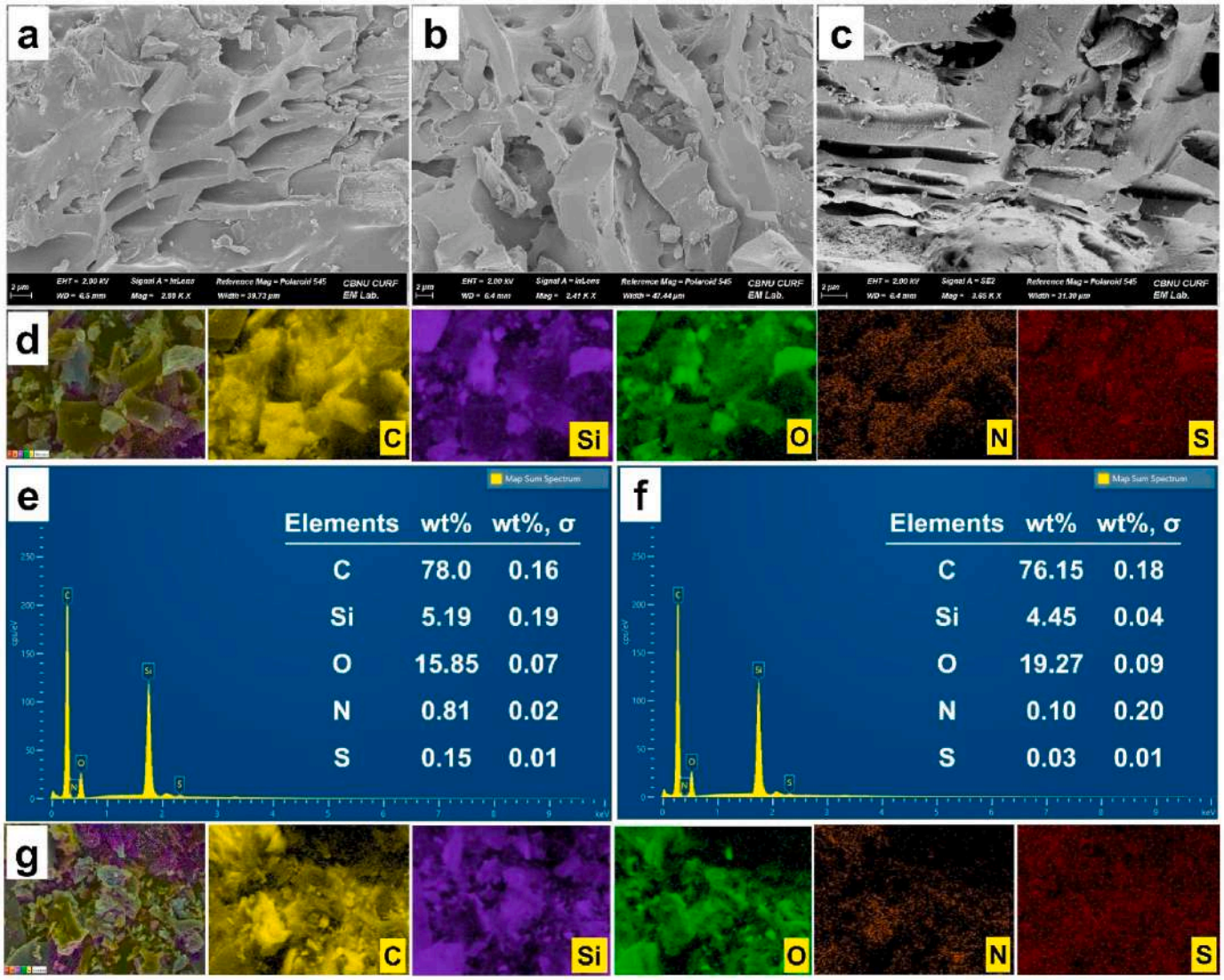

Fig. 7. FESEM images of the (a) initial, (b) used, and (c) regenerated CRH. (d) Element mappings of the used CRH. EDS elemental profiles of the (e) used and (f) regenerated CRH. (g) Element mappings of the regenerated CRH.

Table 5
List of types of regenerating agents for different adsorbents (for MB adsorption) and their regeneration efficiency (% RE) (taken only for first cycle of regeneration).

Adsorbents	Regenerating agents or methods	Regeneration efficiency (%)	Ref.
Cellulose nanofibrils	HCl (0.1 M)	~80.0	Chan et al. (2015)
Iron oxide/SiO_2	Thermal annealing (450 °C/air)	~89.0	Hong et al. (2019)
Iron – activated carbon	H_2SO_4 (0.1 M), $NaNO_3$ (0.01 M) and NaOH (0.1 M)	90 ± 5	Shah et al. (2015)
Silica nanofiber/Fe_3O_4/ porous silica composite	H_2O_2 (30%)/HNO_3 (0.01 M)	96.0	Li et al. (2018)
Michelia figo	Thermal treatment (160 °C/limited air)	~62.0	Guo et al. (2020)
Bentonite clay	Thermo-chemical (160 °C/HCl)	70.0	(Momina et al., 2019)
Sugarcane bagasse-β-cyclodextrin	Ethanol (75%) and HCl (0.1 M)	86.0	Mpatani et al. (2020)
$Mn_{0.6}Zn_{0.4}Fe_2O_4$@SiO_2	H_2O_2 (3 wt%)	94.44	Yu et al. (2021)
NiO/Sepiolite	Thermal treatment (400 °C) with gas (O_2) flow (6L min^{-1})	74.0	Gao et al. (2022)
CRH	CP	~77%	This work

is consistent with the previous literature (Ahmad et al., 2020) as well as the trend observed in the XPS spectra. Given that MB contains N and S whereas CRH does not, the measured N (0.81 wt%) and S (0.15 wt%) signals in Fig. 7(e) are highly likely to arise from the adsorbed MB molecules. On the other hand, decreased N (0.1 wt%) and insignificant S (0.03 wt%) signals were identified after an hour of CP treatment for regeneration of CRH (Fig. 7(f)). This result strongly supports that the adsorbed MB molecules would be removed during CP treatment, and thus the used CRH was successfully regenerated by the oxidation. Also, the reactive oxygen species released during CP treatment brought about a noticeable increase from 15.85 wt% to 19.27 wt% in the O content (Fig. 7(e) and (f)). This information also further supports that the used CRH was oxidized during CP treatment.

3.4. Comparison of the regeneration efficiencies of CP treatment with other regeneration technologies

To weigh up the regeneration capability of CP treatment, we tried to compare the recovered adsorption capacity by CP treatment with the regeneration efficiencies of other approaches such as thermal and chemical regeneration methods. Table 5 shows various kinds of used adsorbents, the regeneration conditions of the used adsorbents, and their regeneration efficiencies at the first cycle. As shown in Table 5, CP treatment was found to be at a moderate level (~77%) as compared to the regeneration efficiencies (62.0%–96.0%) of other regeneration technologies. Such a comparable regeneration efficiency of CP treatment is expected to make CP treatment more readily available for adsorbent regeneration upon consideration that it does not require high energy consumption like thermal regeneration but lessens environmental and operational burdens imposed by the separation and post-treatment of persistently remaining pollutants in cleaning agents used for chemical regeneration. To directly evaluate the actual regeneration effectiveness of CP treatment, we also measured the removal efficiency of the CRH treated by various kinds of regeneration methods in person. According to the result (Fig. 8), the regenerated CRH by CP treatment showed a comparable removal efficiency to that by HCl treatment, while CP treatment was superior to thermal and NaOH treatments. Overall, we believe it is not too much to say that CP treatment is one of the enticing options to recover varieties of adsorbents after MB adsorption.

3.5. Repetitive regeneration of the used CRH by CP treatment

As evidenced by the kinetic study, CP treatment was effective in regenerating used adsorbents. To further verify the regeneration capability of CP treatment during repetitive uses, five adsorption and regeneration cycles were additionally carried out with 0.25 g of CRH and two different concentrations (10 and 20 ppm) of MB solutions. Five consecutive adsorption tests using CRH were also performed without CP treatment to confirm whether the adsorption capability of the used CRH varies depending on CP treatment. As shown in Fig. 9(e), the CRH's removal efficiency of 10 ppm MB dropped from 54.2% to 14.2% at the first reuse without CP treatment and was reduced to 6.8% after five times reuse without CP treatment. It was the case for the removal efficiency of 20 ppm MB, which is evidenced by the fact that the removal efficiency dropped from 50.8% to 9.1% at the first reuse and decreased by 4.4% after five times reuse without CP treatment (Fig. 9(f)). By turns adsorption and CP treatment, however, the regenerated CRH showed a comparable removal efficiency (50.2% and 49.0% for 10 and 20 ppm MB) at the first reuse with CP treatment (Fig. 9(e) and (f)). Also, the removal efficiency was maintained at a moderate level (38.0% and 34.7% for 10 and 20 ppm MB) during five consecutive adsorption tests.

The stark contrast in the adsorption capacity stems from whether the previously adsorbed dye molecules were adequately removed before reuse and thereby adsorption sites were rehabilitated for next use. According to Kim et al. (2022), an adsorption capacity could decrease if the reused adsorbent's adsorption sites were still occupied by previously adsorbed pollutants. Likewise, the used CRH kept losing its adsorption capacity as more adsorption sites were progressively occupied by dye molecules during recurring adsorption without CP treatment. On the other hand, when CP treatment was conducted between the consecutive adsorption tests, the previously adsorbed dye molecules were removed before the next use. As a result, the regenerated CRH revealed a relatively slight decrease in the removal efficiency. The slight reduction in the removal efficiency was estimated to arise from irreversible adsorption. Note that structural deformation is less likely to cause irreversible adsorption in that there were no noticeable damages in the morphologies after five cycles of adsorption and regeneration (Fig. S5). Nevertheless, CP treatment is better than reusing adsorbents without regeneration, considering that CP treatment could further lessen the environmental burden imposed by released pollutants by providing a sustainable way to recycle adsorbents.

Lastly, CP treatment made the adsorption-based water treatment using biochars more energy- and resource-efficient by recycling used CRH. Specifically, the required power consumption to regenerate used CRH by CP treatment was 85 Wh per g CRH. This power consumption is almost negligible upon consideration of the power consumption required to carbonize rice husk to produce CRH (540 Wh g^{-1}), which is necessary when used CRH cannot be reused while having to produce new CRH. Even considering the required energy and resources during harvesting fresh rice husk, their transportation, pre-treatment, *etc.,* the feasibility of CP treatment-based recycling is assumed to be much more highly valued than the simple comparison between the power consumption. In this regard, we could conclude that recycling used biochars by CP treatment is environmentally friendly and practical in that it can enable us to rehabilitate the water environment while recycling resources at low energy and resource consumption. Furthermore, it is worth exploring the regeneration efficiency and economic feasibility of CP treatment at a large scale for future work.

4. Conclusion

In summary, we proposed a novel strategy for the regeneration of carbonized rice husks (CRHs) after the adsorption of MB. Cold plasma

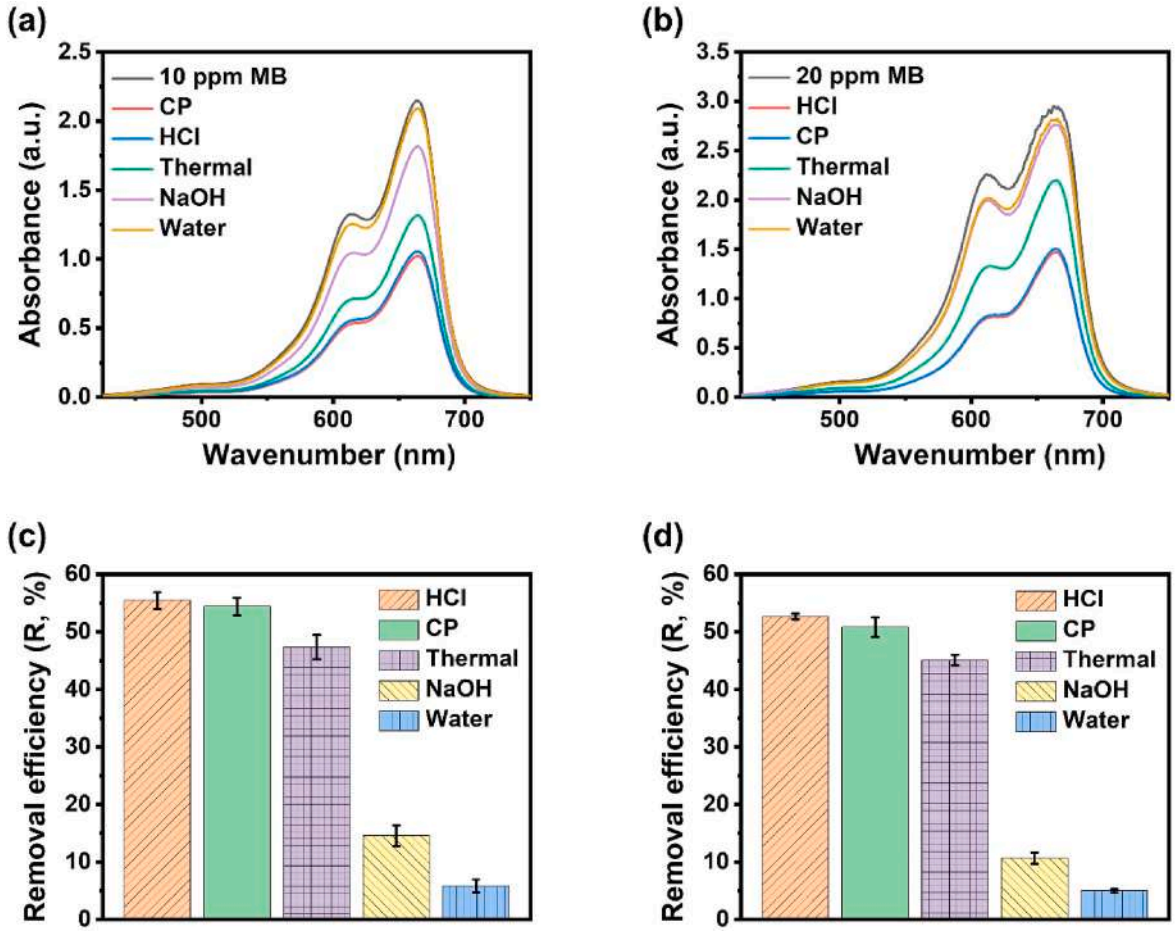

Fig. 8. UV absorbance spectra of adsorption tests using (a) 10 ppm and (b) 20 ppm MB along with the CRH treated by various kinds of regeneration methods. Removal efficiencies of (c) 10 and (d) 20 ppm MB obtained with the CRH treated by various kinds of regeneration methods. For chemical regeneration, 0.1 M HCl and NaOH were used, while thermal regeneration was performed at 100 °C. All the regeneration methods including CP treatment were conducted for 1 h for the comparison.

(CP) treatment showed favorable performance in the regeneration of CRH by generating active radical species capable of removing MB. The calculated Q_e values for initial (5.23 mg g^{-1}), used (1.81 mg g^{-1}), and regenerated (4.03 mg g^{-1}) CRHs suggest the successful recovery of CRH. FTIR, BET, XPS, and EDS analyses demonstrated the regeneration of CRH by CP treatment by revealing that functional groups and elements related to MB disappeared from the used CRH after CP treatment. Thanks to the regeneration by CP treatment, CRH could maintain its removal efficiency at a moderate level (~70% of the initial performance) till the fifth recycle, unlike five consecutive adsorption without CP treatment (~9–13% of the initial performance). The great potential for the adsorbent regeneration was achieved by effectively removing pre-adsorbed MB by CP treatment and rehabilitating adsorption sites. It is also worth noting that the power consumption required to recycle used CRHs by CP treatment was about 6.4 times lower than carbonizing new CRHs, demonstrating the feasibility of recycling biochars by CP treatment. We hope this work could provide insights into an eco-friendly method to regenerate and reuse a variety of adsorbents.

Authorship contribution statement

Dharma Raj Kandel: Data curation, Formal analysis, Investigation, Methodology, Validation, Visualization, Writing - original draft. **Hee-Jun Kim:** Formal analysis, Investigation, Methodology, Validation. **Jeong-Muk Lim:** Formal analysis, Investigation, Methodology, Validation. **Milan Babu Poudel:** Formal analysis, Investigation, Methodology, Validation. **Min Cho:** Formal analysis, Resources, Validation. **Hyun-Woo Kim:** Formal analysis, Resources, Validation. **Byung-Taek Oh:** Formal analysis, Resources, Validation. **Changwoon Nah:** Formal analysis, Resources, Validation. **Seung Hee Lee:** Formal analysis, Resources, Validation. **Bipeen Dahal:** Formal analysis, Validation. **Jaewoo Lee:** Conceptualization, Data curation, Formal analysis, Funding acquisition, Investigation, Project administration, Resources, Supervision, Validation, Visualization, Writing - original draft, Writing - review & editing.

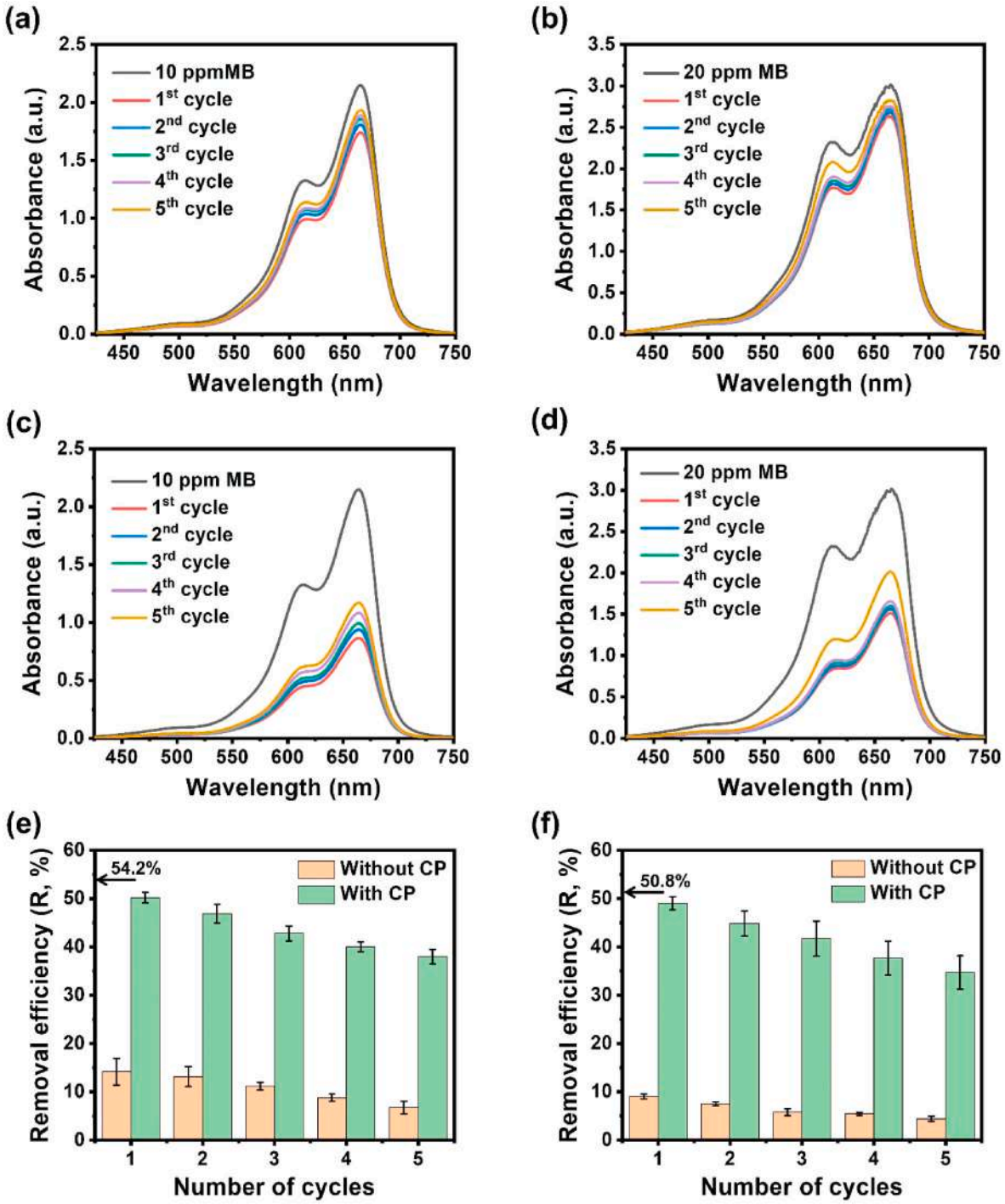

Fig. 9. UV absorbance spectra of consecutive adsorption tests using (a) 10 ppm MB without CP treatment, (b) 20 ppm MB without CP treatment, (c) 10 ppm MB with CP treatment, and (d) 20 ppm MB with CP treatment. Removal efficiencies of (e) 10 and (f) 20 ppm MB depending on CP treatment during consecutive adsorption tests. 54.2% and 50.8% in panels (e) and (f) indicate the initial removal efficiencies for 10 and 20 ppm MB.

Declaration of competing interest

The authors declare that they have no known competing financial interests or personal relationships that could have appeared to influence the work reported in this paper.

Data availability

Data will be made available on request.

Acknowledgement

This work was supported by the Technology development Program (S3249673) funded by the Ministry of SMEs and Startups (MSS, Korea).

Appendix A. Supplementary data

Supplementary data to this article can be found online at https://doi.org/10.1016/j.chemosphere.2022.136638.

References

Adam, F., Appaturi, J.N., Khanam, Z., Thankappan, R., Nawi, M.A.M., 2013. Utilization of tin and titanium incorporated rice husk silica nanocomposite as photocatalyst and adsorbent for the removal of methylene blue in aqueous medium. Appl. Surf. Sci. 264, 718–726.
Ahmad, A., Khan, N., Giri, B.S., Chowdhary, P., Chaturvedi, P., 2020. Removal of methylene blue dye using rice husk, cow dung and sludge biochar: characterization, application, and kinetic studies. Bioresour. Technol. 306, 123202.
Albadarin, A.B., Collins, M.N., Naushad, M., Shirazian, S., Walker, G., Mangwandi, C., 2017. Activated lignin-chitosan extruded blends for efficient adsorption of methylene blue. Chem. Eng. J. 307, 264–272.
Alkaykh, S., Mbarek, A., Ali-Shattle, E.E., 2020. Photocatalytic Degradation of Methylene Blue Dye in Aqueous Solution by MnTiO3 Nanoparticles under Sunlight Irradiation, e03663. Heliyon.
Babu Poudel, M., Shin, M., Joo Kim, H., 2022. Interface engineering of MIL-88 derived MnFe-LDH and MnFe2O3 on three-dimensional carbon nanofibers for the efficient adsorption of Cr(VI), Pb(II), and As(III) ions. Separ. Purif. Technol. 287, 120463.
Bakdash, R.S., Aljundi, I.H., Basheer, C., Abdulazeez, I., 2020. Rice husk derived Aminated Silica for the efficient adsorption of different gases. Sci. Rep. 10, 19526.
Brice, D.N.C., Manga, N.H., Arnold, B.S., Daouda, K., Victoire, A.A., Giresse, N.N.A., Nangah, C.R., Nsami, N.J., 2021. Adsorption of tartrazine onto activated carbon based cola nuts shells: equilibrium, kinetics, and thermodynamics studies. Open J. Inorg. Chem. 11, 1–19.
Brisset, J.L., Pawłat, J., 2015. Chemical effects of air plasma species on aqueous solutes in direct and delayed exposure modes: discharge, post-discharge and plasma activated water. Plasma Chem. Plasma Process. 36, 355–381.
Chan, C.H., Chia, C.H., Zakaria, S., Sajab, M.S., Chin, S.X., 2015. Cellulose nanofibrils: a rapid adsorbent for the removal of methylene blue. RSC Adv. 5, 18204–18212.
Chowdhury, A.K., Sarkar, A.D., Bandyopadhyay, A., 2009. Rice husk ash as a low cost adsorbent for the removal of methylene blue and Congo red in aqueous phases. Clean: Soil, Air, Water 37, 581–591.
Fang, Y., Liu, Q., Zhu, S.J.I.J.o.B.M., 2021. Selective biosorption mechanism of methylene blue by a novel and reusable sugar beet pulp cellulose/sodium alginate/iron hydroxide composite hydrogel. Int. J. Biol. Macromol. 188, 993–1002.
Ferro-Garcia, M., Rivera-Utrilla, J., Bautista-Toledo, M.I., Moreno-Castilla, C., 1996. Chemical and thermal regeneration of an activated carbon saturated with chlorophenols. J. Chem. Technol. Biotechnol. 67, 183–189.
Gao, S., Wang, D., Huang, Z., Su, C., Chen, M., Lin, X., 2022. Recyclable NiO/sepiolite as adsorbent to remove organic dye and its regeneration. Sci. Rep. 12, 2895.
Ghaedi, S., Seifpanahi-Shabani, K., Sillanpää, M., 2022. Waste-to-Resource: new application of modified mine silicate waste to remove Pb2+ ion and methylene blue dye, adsorption properties, mechanism of action and recycling. Chemosphere 292, 133412.
Godlewska, P., Schmidt, H.P., Ok, Y.S., Oleszczuk, P., 2017. Biochar for composting improvement and contaminants reduction. A review. Bioresour. Technol. 246, 193–202.
Guo, D., Li, Y., Cui, B., Hu, M., Luo, S., Ji, B., Liu, Y., 2020. Natural adsorption of methylene blue by waste fallen leaves of Magnoliaceae and its repeated thermal regeneration for reuse. J. Clean. Prod. 267, 121903.
Han, R., Wang, Y., Yu, W., Zou, W., Shi, J., Liu, H., 2007. Biosorption of methylene blue from aqueous solution by rice husk in a fixed-bed column. J. Hazard Mater. 141, 713–718.
Hong, Y., Cha, B.J., Kim, Y.D., Seo, H.O., 2019. Mesoporous SiO2 particles combined with Fe oxide nanoparticles as a regenerative methylene blue adsorbent. ACS Omega 4, 9745–9755.
Hu, S., Xiang, J., Sun, L., Xu, M., Qiu, J., Fu, P., 2008. Characterization of char from rapid pyrolysis of rice husk. Fuel Process. Technol. 89, 1096–1105.
Hummadi, K.K., Luo, S., He, S., 2022. Adsorption of methylene blue dye from the aqueous solution via bio-adsorption in the inverse fluidized-bed adsorption column using the torrefied rice husk. Chemosphere 287, 131907.
Ibrahim, I., Seo, D.H., Angeloski, A., McDonagh, A., Shon, H.K., Tijing, L.D., 2021. 3D microflowers CuS/Sn2S3 heterostructure for highly efficient solar steam generation and water purification. Sol. Energy Mater. Sol. Cells 232, 111377.
Jia, P., Tan, H., Liu, K., Gao, W., 2018. Synthesis, characterization and photocatalytic property of novel ZnO/bone char composite. Mater. Res. Bull. 102, 45–50.
Jun, B.-M., Heo, J., Taheri-Qazvini, N., Park, C.M., Yoon, Y., 2020a. Adsorption of selected dyes on Ti3C2Tx MXene and Al-based metal-organic framework. Ceram. Int. 46, 2960–2968.
Jun, B.-M., Kim, S., Rho, H., Park, C.M., Yoon, Y., 2020b. Ultrasound-assisted Ti3C2Tx MXene adsorption of dyes: removal performance and mechanism analyses via dynamic light scattering. Chemosphere 254, 126827.
Kazemi, M., Taghvaei, H., 2021. A novel multi array dielectric barrier discharge plasma gas diffuser for wastewater treatment: the role of reactive species. Separ. Purif. Technol. 260, 118236.
Kim, H.-J., Lee, U., Kim, H.-W., Cho, M., Lee, J.-W., 2022. Zero discharge of dyes and regeneration of a washing solution in membrane-based dye removal by cold plasma treatment. Membranes 12, 546.
Kim, H.-J., Won, C.-H., Hong, Y.-P., Lee, I.H., Kim, H.-W., 2021. Energy-effective elimination of harmful microcystins by a non-thermal plasma process. Chemosphere 284, 131338.
Kim, H.-J., Won, C.-H., Kim, H.-W., 2020. Optimized pretreatment of non-thermal plasma for advanced sewage oxidation. Int. J. Environ. Res. Publ. Health 17, 7694.
Kim, W.J., Pradhan, D., Min, B.-K., Sohn, Y., 2014. Adsorption/photocatalytic activity and fundamental natures of BiOCl and BiOClxI1−x prepared in water and ethylene glycol environments, and Ag and Au-doping effects. Appl. Catal. B Environ. 147, 711–725.
Küntzel, J., Ham, R.W., Melin, T., 1999. Regeneration of hydrophobic zeolites with steam. Chem. Eng. Technol. 22, 991–994.
Kurbus, T., Slokar, Y.M., Le Marechal, A.M., 2002. The study of the effects of the variables on H2O2/UV decoloration of vinylsulphone dye: part II. Dyes Pigments 54, 67–78.
Lee, D., Lee, J.-C., Nam, J.-Y., Kim, H.-W., 2018. Degradation of sulfonamide antibiotics and their intermediates toxicity in an aeration-assisted non-thermal plasma while treating strong wastewater. Chemosphere 209, 901–907.
Lee, J.-C., Kim, H.-J., Kim, H.-W., Lim, H., 2021. Iron-impregnated spent coffee ground biochar for enhanced degradation of methylene blue during cold plasma application. J. Ind. Eng. Chem. 98, 383–388.
Lee, J., Lim, Y.J., 2021. On the control strategy to improve the salt rejection of a thin-film composite reverse osmosis membrane. Appl. Sci. 11, 7619.
Li, B., Shao, X., Liu, T., Shao, L., Zhang, B., 2016. Construction of metal/WO2.72/rGO ternary nanocomposites with optimized adsorption, photocatalytic and photoelectrochemical properties. Appl. Catal. B Environ. 198, 325–333.
Li, X., Li, C., Goh, K., Chong, T.H., Wang, R., 2022. Layer-by-layer aided β-cyclodextrin nanofilm for precise organic solvent nanofiltration. J. Membr. Sci. 652, 120466.
Li, Z., Tang, X., Liu, K., Huang, J., Peng, Q., Ao, M., Huang, Z., 2018. Fabrication of novel sandwich nanocomposite as an efficient and regenerable adsorbent for methylene blue and Pb (II) ion removal. J. Environ. Manag. 218, 363–373.
Lim, Y.J., Lee, S.M., Wang, R., Lee, J., 2021. Emerging materials to prepare mixed matrix membranes for pollutant removal in water. Membranes 11, 508.
Lu, P.-J., Lin, H.-C., Yu, W.-T., Chern, J.-M., 2011. Chemical regeneration of activated carbon used for dye adsorption. J. Taiwan Inst. Chem. Eng. 42, 305–311.
Lv, J., Zhao, F., Feng, J., Liu, Q., Nan, F., Liu, X., Xie, S., 2020. The impact of particulate and soluble organic matter on physicochemical properties of extracellular polymeric substances in a microalga Neocystis mucosa SX. Algal Res. 51, 102064.
Mahmoudi, F., Saravanakumar, K., Maheskumar, V., Njaramba, L.K., Yoon, Y., Park, C. M., 2022. Application of perovskite oxides and their composites for degrading organic pollutants from wastewater using advanced oxidation processes: review of the recent progress. J. Hazard Mater., 129074
Momina, Rafatullah, M., Ismail, S., Ahmad, A., 2019. Optimization study for the desorption of methylene blue dye from clay based adsorbent coating. Water 11, 1–13.
Mpatani, F.M., Aryee, A.A., Kani, A.N., Guo, Q., Dovi, E., Qu, L., Li, Z., Han, R., 2020. Uptake of micropollutant-bisphenol A, methylene blue and neutral red onto a novel bagasse-β-cyclodextrin polymer by adsorption process. Chemosphere 259, 127439.
Nandi, D., Pulikkalparambil, H., Parameswaranpillai, J., Siengchin, S., 2022. Application of a biowaste of fish (Labeo rohita) scale for the removal of methyl orange from aqueous solutions: optimization of sorption conditions by response surface method and analysis of adsorption mechanism. Biomass Conv. Bioref. 1–12.
Narbaitz, R., Cen, J.J.W.r., 1997. Alternative methods for determining the percentage regeneration of activated carbon. Water Res. 31, 2532–2542.
Narbaitz, R.M., Karimi-Jashni, A., 2009. Electrochemical regeneration of granular activated carbons loaded with phenol and natural organic matter. Environ. Technol. 30, 27–36.
Naushad, M., Alqadami, A.A., AlOthman, Z.A., Alsohaimi, I.H., Algamdi, M.S., Aldawsari, A.M., 2019. Adsorption kinetics, isotherm and reusability studies for the removal of cationic dye from aqueous medium using arginine modified activated carbon. J. Mol. Liq. 293, 111442.
Nemaleu, J.G.D., Kaze, R.C., Tome, S., Alomayri, T., Assaedi, H., Kamseu, E., Melo, U.C., Sglavo, V.M., 2021. Powdered banana peel in calcined halloysite replacement on the setting times and engineering properties on the geopolymer binders. Construct. Build. Mater. 279, 122480.

Ng, S.L., Seng, C.E., Lim, P.E., 2009. Quantification of bioregeneration of activated carbon and activated rice husk loaded with phenolic compounds. Chemosphere 75, 1392–1400.
Nie, L., Goh, K., Wang, Y., Lee, J., Huang, Y., Karahan, H.E., Zhou, K., Guiver, M.D., Bae, T.-H., 2020. Realizing small-flake graphene oxide membranes for ultrafast size-dependent organic solvent nanofiltration. Sci. Adv. 6, eaaz9184.
Panão, C.O., Campos, E.L., Lima, H.H., Rinaldi, A.W., Lima-Tenório, M.K., Tenório-Neto, E.T., Guilherme, M.R., Asefa, T., Rubira, A.F., 2019. Ultra-absorbent hybrid hydrogel based on alginate and SiO2 microspheres: a high-water-content system for removal of methylene blue. J. Mol. Liq. 276, 204–213.
Patawat, C., Silakate, K., Chuan-Udom, S., Supanchaiyamat, N., Hunt, A.J., Ngernyen, Y., 2020. Preparation of activated carbon from Dipterocarpus alatus fruit and its application for methylene blue adsorption. RSC Adv. 10, 21082–21091.
Phan, T.T.V., Bharathiraja, S., Moorthy, M.S., Manivasagan, P., Lee, K.D., Oh, J., 2017. Polypyrrole–methylene blue nanoparticles as a single multifunctional nanoplatform for near-infrared photo-induced therapy and photoacoustic imaging. RSC Adv. 7, 35027–35037.
Poudel, M.B., Awasthi, G.P., Kim, H.J., 2021. Novel insight into the adsorption of Cr(VI) and Pb(II) ions by MOF derived Co-Al layered double hydroxide @hematite nanorods on 3D porous carbon nanofiber network. Chem. Eng. J. 417, 129312.
Poudel, M.B., Yu, C., Kim, H.J., 2020. Synthesis of conducting bifunctional polyaniline@Mn-TiO2 nanocomposites for supercapacitor electrode and visible light driven photocatalysis. Catalysts 10, 546.
Radoor, S., Karayil, J., Jayakumar, A., Nandi, D., Parameswaranpillai, J., Lee, J., Shivanna, J.M., Nithya, R., Siengchin, S., 2022. Adsorption of cationic dye onto ZSM-5 zeolite-based bio membrane: characterizations, kinetics and adsorption isotherm. J. Polym. Environ. 1–14.
Radoor, S., Karayil, J., Jayakumar, A., Parameswaranpillai, J., Siengchin, S., 2021a. An efficient removal of malachite green dye from aqueous environment using ZSM-5 zeolite/polyvinyl alcohol/carboxymethyl cellulose/sodium alginate bio composite. J. Polym. Environ. 29, 2126–2139.
Radoor, S., Karayil, J., Jayakumar, A., Parameswaranpillai, J., Siengchin, S., 2021b. Removal of methylene blue dye from aqueous solution using PDADMAC modified ZSM-5 zeolite as a novel adsorbent. J. Polym. Environ. 29, 3185–3198.
Rethinasabapathy, M., Bhaskaran, G., Park, B., Shin, J.-Y., Kim, W.-S., Ryu, J., Huh, Y.S., 2022. Iron oxide (Fe3O4)-laden titanium carbide (Ti3C2Tx) MXene stacks for the efficient sequestration of cationic dyes from aqueous solution. Chemosphere 286, 131679.
Salvador, F., Martin-Sanchez, N., Sanchez-Hernandez, R., Sanchez-Montero, M.J., Izquierdo, C.J.M., Materials, M., 2015. Regeneration of carbonaceous adsorbents. Part I: thermal regeneration 202, 259–276.
Santoso, E., Ediati, R., Kusumawati, Y., Bahruji, H., Sulistiono, D.O., Prasetyoko, D., 2020. Review on recent advances of carbon based adsorbent for methylene blue removal from waste water. Mater. Today Chem. 16, 100233.
Sethunga, G., Lee, J., Wang, R., Bae, T.-H., 2019a. Influence of membrane characteristics and operating parameters on transport properties of dissolved methane in a hollow fiber membrane contactor for biogas recovery from anaerobic effluents. J. Membr. Sci. 589, 117263.
Sethunga, G.S.M.D.P., Karahan, H.E., Wang, R., Bae, T.-H., 2019b. PDMS-coated porous PVDF hollow fiber membranes for efficient recovery of dissolved biomethane from anaerobic effluents. J. Membr. Sci. 584, 333–342.
Shah, I., Adnan, R., Wan Ngah, W.S., Mohamed, N., 2015. Iron impregnated activated carbon as an efficient adsorbent for the removal of methylene blue: regeneration and kinetics studies. PLoS One 10, 1–23.
Sivakumar, R., Lee, N.Y., 2022. Adsorptive removal of organic pollutant methylene blue using polysaccharide-based composite hydrogels. Chemosphere 286, 131890.
Srivastava, V.C., Mall, I.D., Mishra, I.M., 2008. Adsorption of toxic metal ions onto activated carbon: study of sorption behaviour through characterization and kinetics. Chem. Eng. Process: Process Intensif. 47, 1269–1280.
Toriello, M., Afsari, M., Shon, H.K., Tijing, L.D., 2020. Progress on the fabrication and application of electrospun nanofiber composites. Membranes 10, 204.
Wu, Z., Liao, Q., Chen, P., Zhao, D., Huo, J., An, M., Li, Y., Wu, J., Xu, Z., Sun, B.J.I.J.o.B.M., 2022. Synthesis, characterization, and methylene blue adsorption of multiple-responsive hydrogels loaded with Huangshui polysaccharides, polyvinyl alcohol, and sodium carboxyl methyl cellulose. Int. J. Biol. Macromol. 216, 157–171.
Xing, S., Zhou, Z., Ma, Z., Wu, Y., 2011. Characterization and reactivity of Fe3O4/FeMnOx core/shell nanoparticles for methylene blue discoloration with H2O2. Appl. Catal. B Environ. 107, 386–392.
Yan, K.-K., Huang, J., Chen, X.-G., Liu, S.-T., Zhang, A.-B., Ye, Y., Li, M., Ji, X., 2016. Fixed-bed adsorption of methylene blue by rice husk ash and rice husk/CoFe2O4 nanocomposite. Desalination Water Treat. 57, 12793–12803.
You, X., Wang, R., Zhu, Y., Sui, W., Cheng, D., 2021. Comparison of adsorption properties of a cellulose-rich modified rice husk for the removal of methylene blue and aluminum (III) from their aqueous solution. Ind. Crop. Prod. 170, 113687.
Yu, J., Xu, D., Jiang, D., Xu, C., 2021. Adsorption mechanism of methylene blue from water using core-shell structured magnetic Mn0.6Zn0.4Fe2O4@SiO2 as efficient recyclable adsorbent. Mater. Chem. Phys. 273, 125061.
Zeghioud, H., Nguyen-Tri, P., Khezami, L., Amrane, A., Assadi, A.A., 2020. Review on discharge Plasma for water treatment: mechanism, reactor geometries, active species and combined processes. J. Water Proc. Eng. 38, 101664.
Zhang, X., Shi, P., Zhao, W., Lu, W., Li, F., Min, Y., Xu, Q., 2022. Research on methylene blue degradation based on multineedle-to-plane liquid dielectric barrier discharge mode. Separ. Purif. Technol. 286, 120476.